Generalized Phase Behavior of Small Molecules and Nanoparticles

Guangwen He,[†,‡] Reginald B. H. Tan,[‡,§] Paul J. A. Kenis,[†] and Charles F. Zukoski*,[†]

Department of Chemical & Biomolecular Engineering, University of Illinois at Urbana-Champaign, 600 South Mathews Avenue, Urbana, Illinois 61801, Department of Chemical & Biomolecular Engineering, National University of Singapore, 4 Engineering Drive 4, Singapore 117576, and Institute of Chemical & Engineering Sciences, 1 Pesek Road, Jurong Island, Singapore 627833

Prediction and understanding of the thermodynamic properties and kinetics of phase transitions in molecular systems depends on tuning intermolecular interactions such that the desired structures are assembled. These interactions can depend on the solvent temperature and composition and are difficult to determine in an a priori manner. This is especially true for large and complex molecules and nanoparticles with functionalized surfaces. Here, we demonstrate the use of the pair contribution of the long-time self-diffusivity determined by pulsed-field gradient spin–echo nuclear magnetic resonance as a probe of these interactions. Materials with high solubilities have scaled long-time self-diffusivity, D_2, values that are close to hard sphere values and decrease as the solubility decreases. We find a remarkable correlation between solubility and D_2 for a wide range of hydrogen-bonding solutes that crystallize upon quenching solutions from high temperature. This generalized phase behavior can be understood in terms of the solutes' interacting with attractive forces that have an extent that is only a small fraction of their diameters.

I. Introduction

The assembly of useful structures composed of nanoparticles relies on fine-tuning the interactions between particles. Ordered, disordered, or heterogeneous structures result from a balancing of particle and continuous-phase chemical potentials. Spontaneous structure formation is the result of the suspension sampling local and global free energy minima associated with accessible particle configurations.[1–3] Only recently have engineering methods been developed that enable a priori design of desired structures and thus go beyond the present largely Edisonian, intuitive, or high-throughput screening techniques. One of the first attempts to apply predictive tools comes in the formation of ordered assemblies, or crystals. Prediction of the onset of the ordering transition requires knowledge of the particle interactions derived from ab initio quantum predictions[4,5] or experimental characterization.[6–8] The solvent plays an important role in controlling the strength of interactions, and thus, solubility is difficult to predict in an a priori manner. As a result, experimental methods are often sought to understand how changing solvent composition and temperature will alter the location of the solubility boundary. To date, determination of the osmotic second virial coefficient, measured directly by light scattering[9,10] or indirectly through chromatographic methods,[7,11] has been the main method applied to protein solutions. In this study, we explore an alternative method of characterizing the strength of attraction and that the generalized phase behavior seen in protein solutions extends to molecular solutes.

Globular proteins experience anisotropic interactions and often crystallize into a variety of polymorphs, demonstrating that the effects of specific chemical interactions of the solvent

and other solutes on protein interactions are significant.[12–14] Despite these chemical effects, qualitative understanding of the equilibrium phase behavior and the solvent conditions conducive to protein crystallization can be initiated by treating the proteins as spheres experiencing short-range centrosymmetric interactions that are sensitive to the solvent conditions.[6,9,15–17] This description qualitatively captures the solubility curve and predicts the existence of metastable liquid–liquid-phase separation (LLPS) and the formation of gels.[14] Generalized phase diagrams have been introduced in which the scaled second virial coefficient is used as a Boltzmann-averaged measure of the strength of particle interactions.[6–8] However, the second virial coefficient has not been successful in predicting the location of the metastable liquid–liquid critical point. Anisotropic or valence-limited interactions and nonconformal pair potentials have been suggested as possible explanations.[16,18–20]

Three outcomes of these prior studies are of significance to the current work. First, the effect of solvent composition on the strength of solute interactions is substantial. As a result, in the assembly of nanoparticles into desired structures, the composition of the continuous phase can be considered as a design tool. Second, the techniques for characterizing the strength of interactions based on the second virial coefficients require relatively large quantities of nanoparticles, whereas the methods tend to be tedious to implement. Both of these points suggest the need for alternate, facile methods for characterizing the particle interactions. The third conclusion to be drawn from the qualitative success of simple fluid theories in predicting the phase diagrams for complex molecules such as proteins lies in the lack of absolute molecular size dependence of these models.[15,21,22] In this study, we expand on these observations to show that fluid models are useful in understanding solubility of solutes ranging from biomacromolecules to low-molecular-weight organic molecules.

* To whom correspondence should be addressed. E-mail: czukoski@uiuc.edu.
† University of Illinois.
‡ National University of Singapore.
§ Institute of Chemical & Engineering Sciences.

Phase Behavior of Small Molecules, Nanoparticles

J. Phys. Chem. B, Vol. 111, No. 43, 2007 **12495**

TABLE 1: Solvent Compositions and Temperatures Used for the Self-Diffusivity Measurement of Different Solutes Used in This Study[a]

solute	solvent compositions (temperature in °C)	mol diam (nm)
glycine	H_2O (5, 25, 40, 75); 18/82 w% IPA/H_2O (25); 31/69 w% IPA/H_2O (25)	0.48
L-histidine	H_2O (25, 60)	0.63
L-phenylalanine	H_2O (25)	0.66
paracetamol	50/50 w% Acetone/H_2O (20, 25, 30); 70/30 w% Acetone/H_2O (20, 25, 30)	0.64
ibuprofen	50/50 w% EtOH/H_2O (10, 15, 20, 25); 60/40 w% EtOH/H_2O (10, 15, 20, 25); 70/30 w% EtOH/H_2O (15, 20, 25, 30); 80/20 w% EtOH/H_2O (15, 20, 25, 30); EtOH (15, 20, 25)	0.76
hen egg white lysozyme	0.1M NaAc, pH = 4.5, and 3 w/v% NaCl (20, 25, 30); 0.1M NaAc, pH = 4.5, and 5 w/v% NaCl (25, 30, 35)	3.02

[a] The sizes of the molecules are estimated as described in the text.

In seeking facile experimental methods to characterize particle interactions for relatively small organic molecules, such as amino acids and pharmaceutical compounds, we find that the second viral coefficient, B_2, is difficult to measure. Instead, we decided to use the pair contribution of the long-time self-diffusivity determined by pulsed-field gradient spin–echo nuclear magnetic resonance (PGSE NMR) as a probe of particle interactions. The molecular diffusivity is determined by the attenuation of a spin–echo signal resulting from the combinatory effect of the translational motion of nuclear spins and the impositions of spatially well-defined gradient pulses.[23] This method proves useful in that the signal is specific to the molecule of interest such that any signal measured is not cross-contaminated by the presence of other molecules, as would occur, for example, in light scattering measurements in mixtures of objects of similar size.

Below in Section II, we describe the experimental technique we have implemented, and in Section III, we explore the theoretical links between the long-time self-diffusivity and the strength of solute. This approach shows that the pair contribution of the scaled long-time self-diffusivity, D_2, is sensitive to the strength and range of the particle interactions. With this knowledge, we explore how particle solubility changes with the strength and range and thus how we might expect changes in D_2 to be reflected in changes in solubility. In Section IV, we present experimental results for the concentration dependence of self-diffusivity and develop a generalized phase diagram in which D_2 is used as an experimentally measurable quantity to estimate the effective strength of solute interactions. In Section V, we draw conclusions.

II. Experimental Section

Materials. Various solute molecules [the amino acids glycine (Fluka, >99.5%), L-histidine (Fluka, >99.5%) and L-phenyla-lanine (Sigma, >98.5%), the pharmaceuticals paracetamol (Sigma, >98%) and ibuprofen (Fluka, >99%), and the protein hen egg white lysozyme (Sigma, 3× recrystallized)] were dissolved into different solvents [deionized water (Barnstead, E-pure, 18 MΩ-cm), ethanol (AAPER alcohol, absolute 200 proof), isopropyl alcohol (Sigma, >99.5%, A.C.S. reagent), acetone (Sigma, >99.5%, A.C.S. reagent), and sodium acetate buffer (0.1 M, pH = 4.5) made by dissolving an appropriate amount of sodium acetate (Fluka, certified A.C.S. anhydrous) into a mixture of deionized water and acetic acid (Fisher Scientific, A.C.S. Reagent) in the presence of sodium chloride (Fluka, Certified A.C.S.)] or solvent mixtures at different temperatures. All chemicals are used without further purification. Detailed solution compositions and experimental conditions are summarized in Table 1.

Measurement of Self-Diffusivity Using Nuclear Magnetic Resonance (NMR). The long-time self-diffusivities of various molecules in different solvents were measured using ^{1}H PGSE NMR (time scale: 1500 ms) with a 600 MHz spectrometer (Varian Unity Inova 600). A special sampling setup was implemented in our experiments (Figure 1). The sample solution was injected to a spherical bulb microcell (Wilmad Glass, 5 mm) and then inserted into an NMR tube (Wilmad Glass, 5 mm) filled with D_2O (Sigma, Standard 99.98 ± 0.01 atom % D). This setup offers two advantages: (i) strong magnetic signals from the protonated molecules in the solvent (due to the use of ^{1}H probe) can be greatly reduced and (ii) material consumption can be minimized. Prior to each set of experiments at different temperatures, the NMR probe was calibrated using reported self-diffusion coefficients of water at respective temperatures.[24–26]

III. Linking Experiments To Theory

Equilibrium Thermodynamic Model. The theoretical approaches used to study the phase behavior of molecular solutions are analogous to those used in liquid-state physics.[27] A commonly used interaction potential of simple fluids is the square well potential that successfully captures the essence of both the repulsive and the attractive natures of the interaction yet maintains remarkable mathematical simplicity. The square well potential can be expressed as follows:

$$u(r) = \begin{cases} \infty & r < 2 \\ -\epsilon & 2 \leq r < 2\lambda \\ 0 & r \geq 2\lambda \end{cases} \quad (1)$$

where r is the center-to-center distance of separation between the particles normalized by the radius of particle a, and ϵ and λ are the strength and range of interaction, respectively. The square well potential was chosen as a model in this study
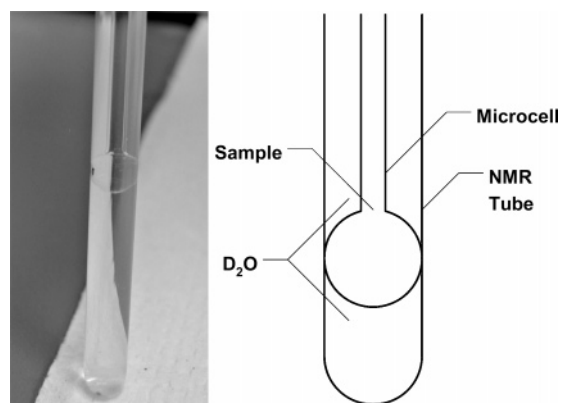

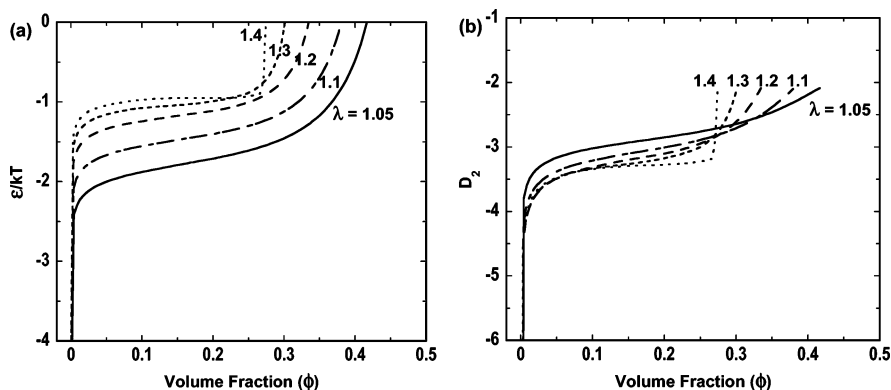**Figure 1.** The sample setup in PGSE NMR self-diffusion experiments.

12496 *J. Phys. Chem. B, Vol. 111, No. 43, 2007*

He et al.

Figure 2. Phase diagrams showing solubility boundaries for different ranges of interaction λ: (a) ϵ/kT as a function of ϕ and (b) D_2 as a function of ϕ.

because the theoretical correlations of thermodynamic and transport properties of the square well fluids with the particle interactions have been well-established in the literature.[21,28−31] The near quantitative agreement between predicted and measured solubilities observed for a variety of nanoparticles and proteins suggests that a simple fluid model such as the square well potential captures many fundamental features of nanoparticle phase behavior. Ramakrishnan and Zukoski[31] developed an equation of state for square well fluids based on the work of Heyes and Aston,[30]

$$Z = \frac{4\pi P a^3}{3\phi kT} = 1 + \frac{b\phi}{(1 - \phi/\phi_0)^2} + \frac{6\phi(\epsilon/kT)f(\lambda)}{\pi(1 - \phi/\phi_b)^3} \quad (2)$$

where Z is the compressibility factor, P is the osmotic pressure, k is the Boltzmann constant, T is the absolute temperature, ϕ is the particle volume fraction, $b = 4\pi/3$ and $\phi_0 = 0.8404$, and $f(\lambda)$ and ϕ_b are tabulated functions of λ.[31] Following Lomakin et al.[32] and Asherie et al.,[21] the chemical potentials of the particles in the liquid phase and solid phase can be calculated by eqs 3 and 4, respectively,

$$\mu_l = \int_0^\phi \left(\frac{4\pi P a^3}{3\phi' kT} - 1\right)\frac{d\phi'}{\phi'} + \frac{4\pi P a^3}{3\phi kT} + \ln(\phi) - 1 \quad (3)$$

$$\mu_s = -\frac{n_s}{2}\left(\frac{\epsilon}{kT}\right) - 3\ln(\lambda - 1) \quad (4)$$

where n_s is the number of nearest neighbors in the solid and that is taken as 12 for face-centered cubic solids.[21]

The metastable liquid−liquid phase boundary can be found by solving equations of mechanical and chemical equilibria of the two liquid phases I and II simultaneously, in which $P^I = P^{II}$ and $\mu^I = \mu^{II}$. If the solid phase is considered to be incompressible, equating μ_l and μ_s gives the solid−liquid phase boundary (solubility), that is, the equilibrium solubility. Finally, phase diagrams showing the strength of interaction ϵ/kT as a function of particle volume fraction ϕ for different ranges of interaction, λ, can be generated (Figure 2a).

Molecular Self-Diffusion. The classical theory of Brownian motion deals with the random movement of an individual solute particle due to stochastic collisions with the solvent molecules of the surrounding fluid. In the dilute limit, the long-time self-diffusivity of the molecule of interest in a continuum, D_s, can be written as[33−36]

$$\frac{D_s}{D_0} = 1 + D_2'c + O(c^2) = 1 + D_2\phi + O(\phi^2) \quad (5)$$

where D_0 is the Stokes−Einstein diffusivity and c and ϕ are, respectively, the absolute concentration and the volume fraction of solute that are linked by $\phi = c(N_A/M_w)(4\pi a^3/3)$. The pair contribution of the scaled self-diffusivity, D_2, can be expressed as $D_2'(N_A/M_w)(4\pi a^3/3)$, where N_A, M_w, and a are Avogadro's number, the molecular weight, and the radius of the solute particle, respectively. In the continuum limit, the long-time self-diffusivity of identical spherical particles has been well-studied such that D_2 can be expressed as[33−36]

$$D_2 = \int_2^\infty (-3 + A_{11} + 2B_{11})\, g(r)r^2\, dr +$$
$$\int_2^\infty \left[\frac{A_{11} - A_{12} - B_{11} + B_{12}}{r} + \frac{1}{2}\left(\frac{dA_{11}}{dr} - \frac{dA_{12}}{dr}\right)\right] Q(r)\, g(r)r^2\, dr \quad (6)$$

The first integral is the first-order correction in the short-time self-diffusivity; the second integral is the long-time correction due to the modification of the pair distribution function of the interacting Brownian particles. In eq 6, $Q(r)$ characterizes the perturbation of the Maxwell−Boltzmann form of the pair distribution function due to forces applied to the particles. Values of $Q(r)$ as well as of the mobility functions A_{11}, A_{12}, B_{11}, and B_{12} are known in the hydrodynamic limit.[35,37] Detailed simulation studies indicate that the continuum model used above is an accurate description of solute diffusivity as long as solutes are on the order of, if not larger than, the size of the solvent.[33,34,38] In the dilute limit, the pair correlation function $g(r)$ is written as[27]

$$g(r) = \exp[-u(r)/kT] \quad (7)$$

Now, D_2 can be calculated as a function of ϵ/kT for given values of λ from eqs 1, 6, and 7. And finally, we can convert the phase diagram of ϵ/kT as a function of particle volume fraction ϕ (Figure 2a) to a D_2 phase diagram (Figure 2b).

For the case in which the identical particles behave like impenetrable hard spheres (i.e., $\epsilon = 0$), Batchelor calculated D_2 to be -2.1,[34] and this value has been adapted widely since. Figure 2a shows that ϵ/kT at the solubility boundary changes with λ; however, such variations are much more subtle when D_2 is used as the measure of strength of interaction (Figure 2b), which echoes the literature findings of a corresponding-states solubility behavior of protein solutions when the osmotic second virial coefficient B_2 is used to characterize the strength of interaction.[15,16] When the particles are interacting via short-range interactions ($\lambda < 1.3$), these variations are negligible. This result also agrees with the simulation studies of Sciortino and co-
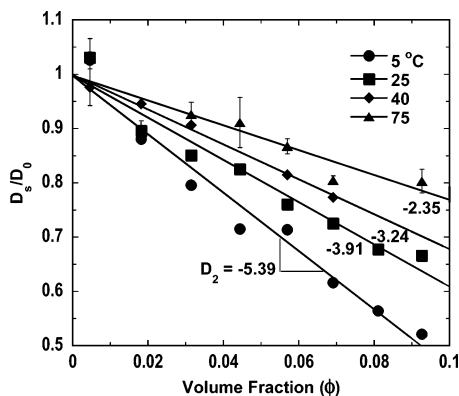
Phase Behavior of Small Molecules, Nanoparticles

J. Phys. Chem. B, Vol. 111, No. 43, 2007 **12497**

Figure 3. Scaled long-time self-diffusivities of glycine in H_2O as a function of solute particle volume fraction at different temperatures. The slopes of the linear fits provide values for D_2. Some error bars are smaller than the size of the symbols.

workers,[39−41] showing that for short-range attractions, thermodynamic and diffusive properties are strongly coupled. Note that for D_2 values for very soluble materials (solubility >0.2 in terms of particle volume fraction), we find that D_2 is insensitive to solubility and takes on a measured value of -2.1 ± 0.2. For a square well with $\lambda = 1.1$, this corresponds to $0 > \epsilon/kT > -1$. Note also that if any changes in the solution compositions and temperature leading to stronger attraction between solute particles, that is, a decrease in solubility, the value of D_2 drops below the hard sphere limit. Thus, D_2 is always negative.

IV. Results And Discussion

For the molecules of interest, the self-diffusivity is a linear function of solute concentration over a wide range of concentrations and is sensitive to temperature (Figure 3). With a drop in temperature, D_2 becomes more negative, indicating an increase in the strength of attraction. Extrapolating to zero concentration diffusivity in a plot of self-diffusivity as a function of the volume fraction ϕ provides a measure of D_0. Note also that the value of D_2 is sensitive to the choice of particle radius, a, since D_2 can be written as $D_2'(N_A/Mw)(4\pi a^3/3)$. As a first choice of particle radius, we can assume that the solute is suspended in a continuous phase of viscosity η and that the Stokes−Einstein expression $D_0 = kT/\xi\eta a$ holds. The hydrodynamic boundary conditions to be applied result in uncertainty in particle size, since ξ equals 6π and 4π for no-slip and slip boundary conditions, respectively. Due to this and other sources of uncertainty introduced by using the Stokes−Einstein expression, we instead estimate the molecular volume in the crystalline phase as $M_v = M_w/\rho_{cr}N_A$, where M_w is the molecular weight of the molecule, ρ_{cr} is the density of crystals, and N_A is Avogadro's number. The molecular volumes estimated by this means can be treated as the sum of the actual molecular volume that the molecules take up, M_v', and the void space in the crystal. However, the actual void fraction of molecular crystals is far more complicated as compared to atomic crystals that display standard packing patterns, such as simple cubic, body-centered cubic, face-centered cubic (FCC), hexagonal-closed packed (HCP), etc. We find that for very soluble materials, the volume fractions of liquid phases calculated from M_v can exceed 0.74. As a result, we seek a systematic and unambiguous way of linking crystal density to a molecular size. In keeping with the model developed above, we determine a molecular size from M_v assuming the particles are spherical and closely packed in an FCC or HCP lattice with volume fractions of 0.74, that is,

$M_v' = 0.74M_v$. The particle size is calculated from M_v' assuming the molecule is spherical in shape. Our choice is made to provide an experimental molecular size such that the comparisons we make between different solutes and solvents do not require interpretation through models. We emphasize that the qualitative results of this paper are independent of choice of a consistent particle size, a.

Solubilities of the molecules studied here are presented in Figure 4. Values of D_2 of both small and large molecules are sensitive to particle type, temperature, and solvent composition. However, when the particle interactions are short-ranged, these D_2 values fall within a narrow range at the same solubility, despite the chemical differences of the molecules investigated. This finding is consistent with the B_2 studies in which broad classes of globular molecules display a common solubility if the particle interactions are short in range.[15] Note that the experimentally derived D_2 values are -2.1 ± 0.2 in the limit of high solubility and are insensitive to solubility until the solubility has dropped below $\phi = 0.2$ as predicted by simple fluid models. This compilation of solubilities demonstrates that (i) when compared at similar strengths of attraction, the solutions of the molecules studied here have very similar equilibrium phase behavior, demonstrating the usefulness of D_2 as a tool for locating solubility boundaries; and (ii) applicability of these generalized phase diagrams extends from systems with biomacromolecules to those with small molecules. In a recent simulation study, Mittal et al. demonstrated a quantitative link between self-diffusivity and excess entropy.[42] The excess entropy is related to other thermodynamic functions, such as the pair correlation function, $g(r)$, and thus may provide an explanation for why we see such a good correlation between D_2 and solubility. Simulation studies by Lekkerkerker and co-workers on phase behavior of rod−sphere mixtures have shown that even with a large aspect ratio of 20, the shapes of the phase diagrams are not too much different from those of the hard spheres, implying that our generalized phase diagram in the D_2 space might be extended to the study of nonideally spherical model systems.[43,44]

We note that the phase diagram is unable to predict formation of multiple polymorphs upon solid−liquid phase transition due to the limitations of the simple fluid theories. Nevertheless, the simple fluid theory captures the solubility in a semiquantitative manner. Note also that the solubility boundaries calculated from different ranges of attraction, λ, collapse into a narrow range for $\lambda < 1.3$ (Figure 2b), thus predicting λ for the interacting solute particles from the solubility data or D_2 is not advisable. On the other hand, this insensitivity of solubility subject to the change in range of attraction also indicates that the thermodynamics of solutions near crystallization depends mainly on the short nature of the interaction potential, regardless of the details of the interaction.

Although LLPS as well as gel formation commonly occurs in protein solutions, these states are rarely seen in small molecule solutions. Detailed calculations show that LLPS becomes metastable relative to the solid−liquid phase boundary as the range of attraction λ becomes smaller than ~ 1.3.[45] Recent studies for short-range attractions suggest that anisotropy in the pair interaction potentials can alter the volume fraction and the strength of attraction at the critical point.[16,18−20] In addition, the complete absence of a metastable LLPS may arise due to a fast crystal nucleation rate.[13] The fact that small molecules appear to exhibit phase behavior similar to that of globular proteins offers new insights for where to look for metastable states in small molecule solutions.
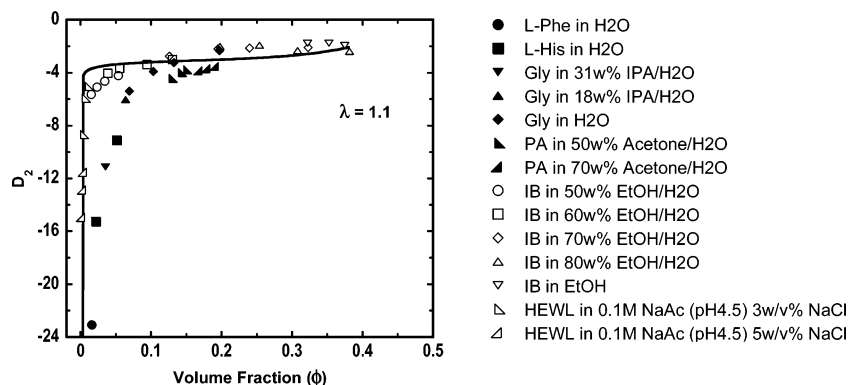
12498 *J. Phys. Chem. B, Vol. 111, No. 43, 2007*

He et al.

Figure 4. Phase diagram for a variety of solutes in D_2 space. The different symbols correspond to experimental data obtained for molecular systems as specified in Table 1. Solubility data for various systems are obtained from the literature,[46−50] then converted to volume fraction as described in the text. The solid line is the model solid−liquid phase boundary for range of interaction λ of 1.1.

V. Conclusion

In this work, we demonstrate the success in using D_2 as a reasonable predictor of the solubility of small hydrogen-bonding molecules. A comparison with the phase behavior of lysozyme indicates that only modest differences exist in the effective interactions of weakly to modestly soluble small molecules and those of nanoparticles. Comparison of the solubility behavior of such broad classes of materials suggests that the interactions dominating the fluid-solid phase behavior have a range that is small compared to the molecular size.

Nucleation and growth of protein crystals has been extensively studied, providing insights on the mechanisms of fluid−solid phase transitions and the origins of metastable states. The small molecules studied here form hydrogen bonds in the solid state that are highly directional and have a range of 0.2−0.3 nm such that λ is expected to be on the order of 1.2−1.5. These estimates are at the edge of, but larger than, attractive well widths that will show stable LLPS for spheres interacting with isotropic square-well attractions. We note, however, that these systems are valance-limited and have strongly isotropic interactions, suggesting that these factors may suppress the critical point to lie below the solubility boundary. In sum, our studies indicate that the equilibrium behavior of small and large molecules is very similar when compared on the same basis, suggesting that advances made in understanding the equilibrium phase behavior of globular protein solutions can be applied to a wide variety of molecular and colloidal systems.

References and Notes

(1) Davey, R. J. *Nature* **2004**, *428*, 374−375.
(2) Lin, Y.; Böker, A.; He, J.; Sill, K.; Xiang, H.; Abetz, C.; Li, X.; Wang, Y.; Emrick, T.; Long, S.; Wang, Q.; Balazs, A.; Russell, T. P. *Nature* **2005**, *434*, 55−59.
(3) Thornton, G. *Science* **2003**, *300*, 1378−1379.
(4) Buttar, D.; Charlton, M. H.; Docherty, R.; Starbuck, J. *J. Chem. Soc., Perkin Trans. 2* **1998**, 763−772.
(5) Mirmehrabi, M.; Rohani, S. *J. Pharm. Sci.* **2005**, *94*, 1560−1576.
(6) Neal, B. L.; Asthagiri, D.; Lenhoff, A. M. *Biophys. J.* **1998**, *75*, 2469−2477.
(7) Tessier, P. M.; Lenhoff, A. M.; Sandler, S. I. *Biophys. J.* **2002**, *82*, 1620−1631.
(8) Mirarefi, A. Y.; Zukoski, C. F. *J. Cryst. Growth* **2004**, *265*, 274−283.
(9) George, A.; Wilson, W. W. *Acta Crystallogr. D* **1994**, *50*, 361−365.
(10) Guo, B.; Kao, S.; Asanov, A.; Combs, L. L.; Wilson, W. W. *J. Cryst. Growth* **1999**, *196*, 424−433.
(11) Tessier, P. M.; Vandrey, S. D.; Berger, B. W.; Pazhianur, R.; Sandler, S. I.; Lenhoff, A. M. *Acta Crystallogr. D* **2002**, *58*, 1531−1535.
(12) Vekilov, P. G. *Methods Enzymol.* **2003**, *368*, 84−105.
(13) Vekilov, P. G. *Cryst. Growth Des.* **2004**, *4*, 671−685.
(14) Kulkarni, A. M.; Dixit, N. M.; Zukoski, C. F. *Faraday Discuss.* **2002**, *123*, 37−50.
(15) Rosenbaum, D.; Zamora, P. C.; Zukoski, C. F. *Phys. Rev. Lett.* **1996**, *76*, 150−153.
(16) Katsonis, P.; Brandon, S.; Vekilov, P. G. *J. Phys. Chem. B* **2006**, *110*, 17638−17644.
(17) Ruppert, S.; Sandler, S. I.; Lenhoff, A. M. *Biotechnol. Prog.* **2001**, *17*, 182−187.
(18) Sear, R. P. *J. Chem. Phys.* **1999**, *111*, 4800−4806.
(19) Kern, N.; Frenkel, D. *J. Chem. Phys.* **2003**, *118*, 9882−9889.
(20) Zaccarelli, E.; Saika-Voivod, I.; Moreno, A. J.; Nave, E. L.; Buldyrev, S. V.; Sciortino, F.; Tartaglia, P. *J. Phys.: Condens. Matter* **2006**, *18*, S2373−S2382.
(21) Asherie, N.; Lomakin, A.; Benedek, G. B. *Phys. Rev. Lett.* **1996**, *77*, 4832−4835.
(22) Noro, M. G.; Frenkel, D. *J. Chem. Phys.* **2000**, *113*, 2941−2944.
(23) Price, W. S. *Concepts Magn. Reson.* **1997**, *9*, 299−336.
(24) Millis, R. *J. Phys. Chem.* **1973**, *77*, 685−688.
(25) Easteal, A. J.; Price, W. E.; Woolf, L. A. *J. Chem. Soc., Faraday Trans. 1* **1989**, *85*, 1091−1097.
(26) Holz, M.; Heil, S. R.; Sacco, A. *Phys. Chem. Chem. Phys.* **2000**, *2*, 4740−4742.
(27) Hansen, J. P.; McDonald, I. R. *Theory of Simple Liquids*, 3rd ed.; Academic Press: London, 2006.
(28) Henderson, D.; Scalise, O. H.; Smith, W. R. *J. Chem. Phys.* **1980**, *72*, 2431−2438.
(29) Vega, L.; De Miguel, E.; Rull, L. F.; Jackson, G.; McLure, I. A. *J. Chem. Phys.* **1991**, *96*, 2296−2305.
(30) Heyes, D. M.; Aston, P. J. *J. Chem. Phys.* **1992**, *97*, 5738−5748.
(31) Ramakrishnan, S.; Zukoski, C. F. *J. Chem. Phys.* **2000**, *113*, 1237−1248.
(32) Lomakin, A.; Asherie, N.; Benedek, G. B. *J. Chem. Phys.* **1996**, *104*, 1646−1656.
(33) Batchelor, G. K. *J. Fluid Mech.* **1976**, *74*, 1−29.
(34) Batchelor, G. K. *J. Fluid Mech.* **1983**, *131*, 155−175.
(35) Cichocki, B.; Felderhof, B. U. *J. Chem. Phys.* **1988**, *89*, 3705−3709.
(36) Cichocki, B.; Felderhof, B. U. *J. Chem. Phys.* **1990**, *93*, 4427−4432.
(37) Jeffrey, D. J.; Onishi, J. *J. Fluid Mech.* **1984**, *139*, 261−290.
(38) Bosma, J. C.; Wesselingh, J. A. *Trans. IChemE, Part A* **1999**, *77*, 325−328.

(39) Foffi, G.; De Michele, C.; Sciortino, F.; Tartaglia, P. *Phys. Rev. Lett.* **2005**, *94*, 078301.1−078301.4.

(40) De Michele, C.; Gabrielli, S.; Tartaglia, P.; Sciortino, F. *J. Phys. Chem. B* **2006**, *110*, 8064−8079.

(41) De Michele, C.; Tartaglia, P.; Sciortino, F. *J. Chem. Phys.* **2006**, *125*, 204720.1−204710.8.

(42) Mittal, J.; Errington, J. R.; Truskett, T. M. *J. Phys. Chem. B* **2006**, *110*, 18147−18150.

(43) Vliegenthart, G. A.; Lekkerkerker, H. N. W. *J. Chem. Phys.* **1999**, *111*, 4153−4157.

(44) Aarts, D. G. A. L.; Tuinier, R.; Lekkerkerker, H. N. W. *J. Phys.: Condens. Matter* **2002**, *14*, 7551−7561.

(45) Hagen, M. H. J.; Frenkel, D. *J. Chem. Phys.* **1994**, *101*, 4093−4097.

(46) Fasman, G. D., Ed.; *Handbook of Biochemistry and Molecular Biology*; CRC Press: Cleveland, 1975; Physical and Chemical Data, Vol. I.

(47) http://www.ajinomoto.co.jp/amino/e_aminoscience/bc/amino_08.html (Date accessed: 2005−12-31).

(48) Granberg, R. A.; Rasmuson, Å. C. *J. Chem. Eng. Data* **2000**, *45*, 478−483.

(49) Khalifeh, I. *Thermodynamic Evaluation of Ibuprofen Solubility in Aqueous and Non-Aqueous Cosolvent Systems*. Ph.D. Thesis, Purdue University, 2000.

(50) Forsythe, E. L.; Judge, R. A.; Pusey, M. L. *J. Chem. Eng. Data* **1999**, *44*, 637−640.